

Supporting information for:

Resonances of the anthracenyl anion probed by frequency-resolved photoelectron imaging of collision-induced dissociated anthracene carboxylic acid

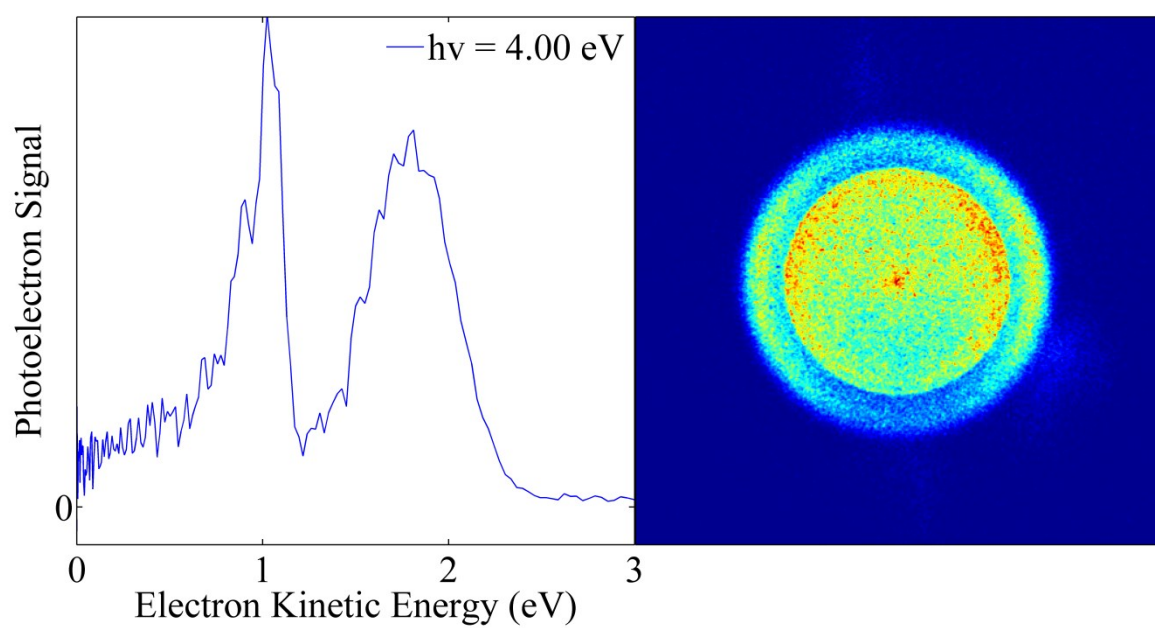
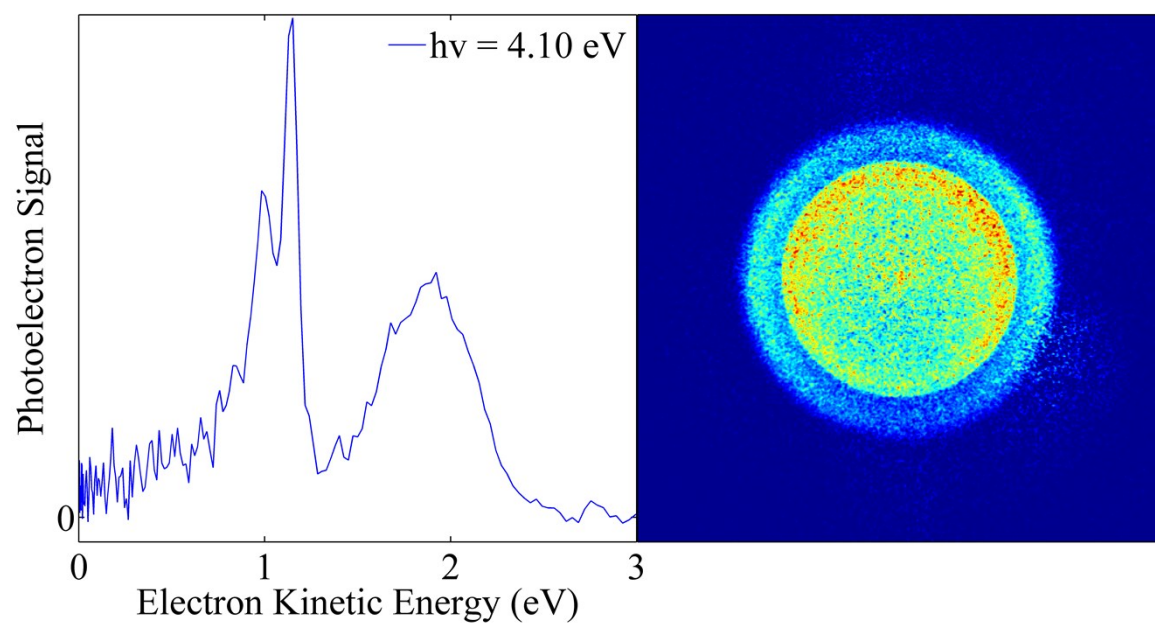
Laurence H. Stanley,^a Cate S. Anstöter^a and Jan R. R. Verlet^{a†}

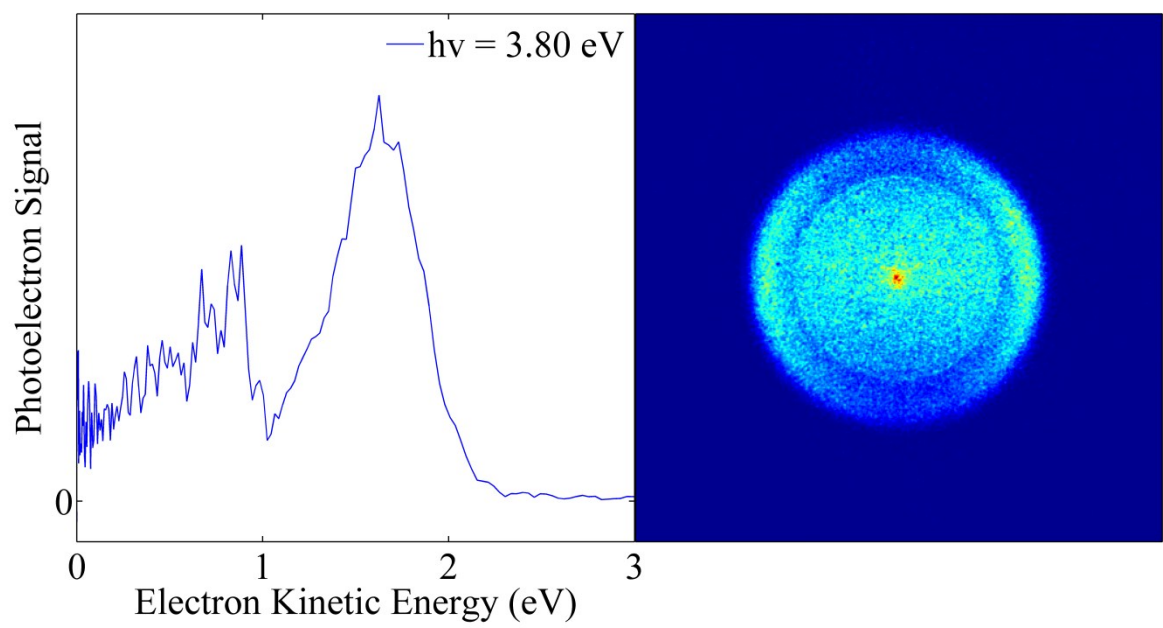
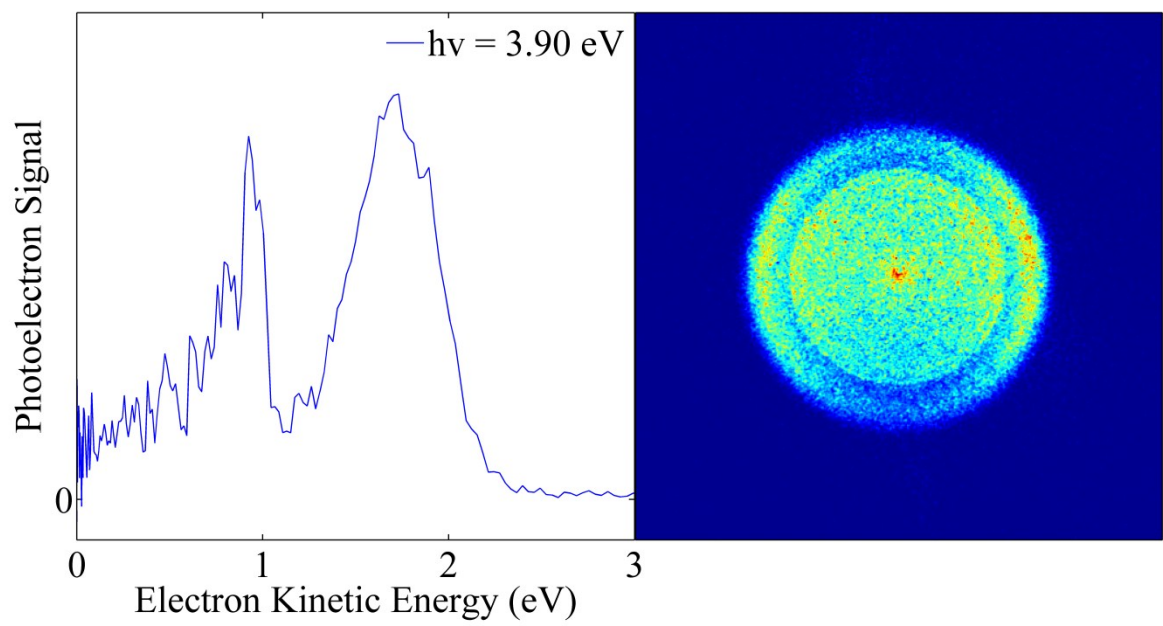
Individual photoelectron spectra and raw photoelectron images	Pages 2-12
Photoelectron spectra of fragment from 9- and 1-C₁₄H₉-CO₂⁻ precursor	Page 13
Excited state molecular orbital contributions for from 9-C₁₄H₉⁻ precursor	Page 14

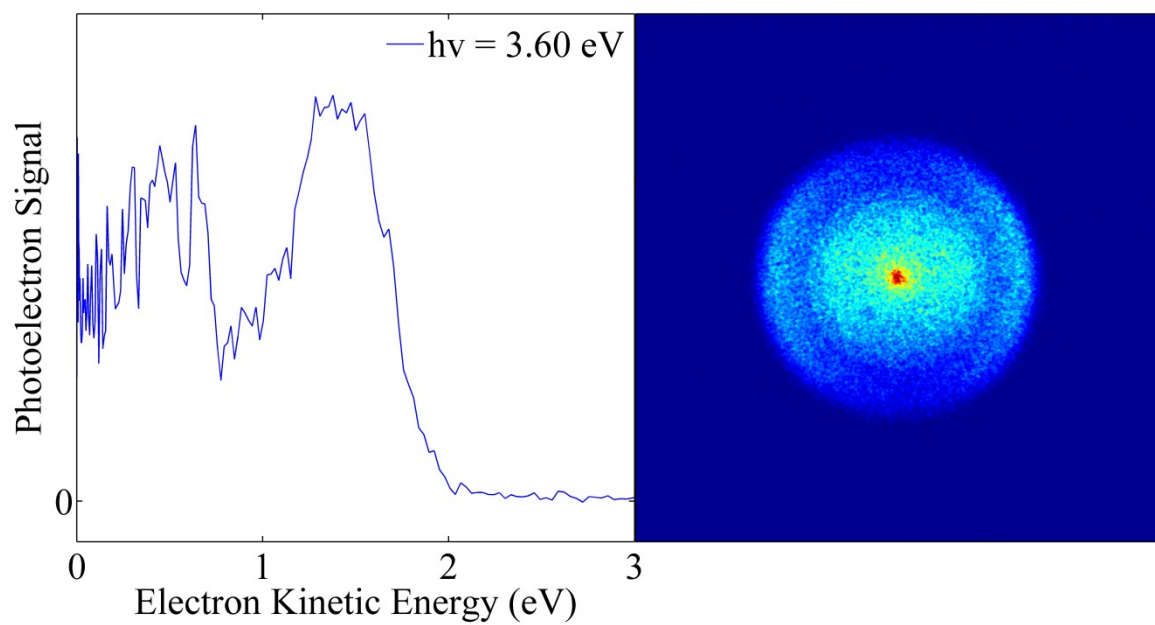
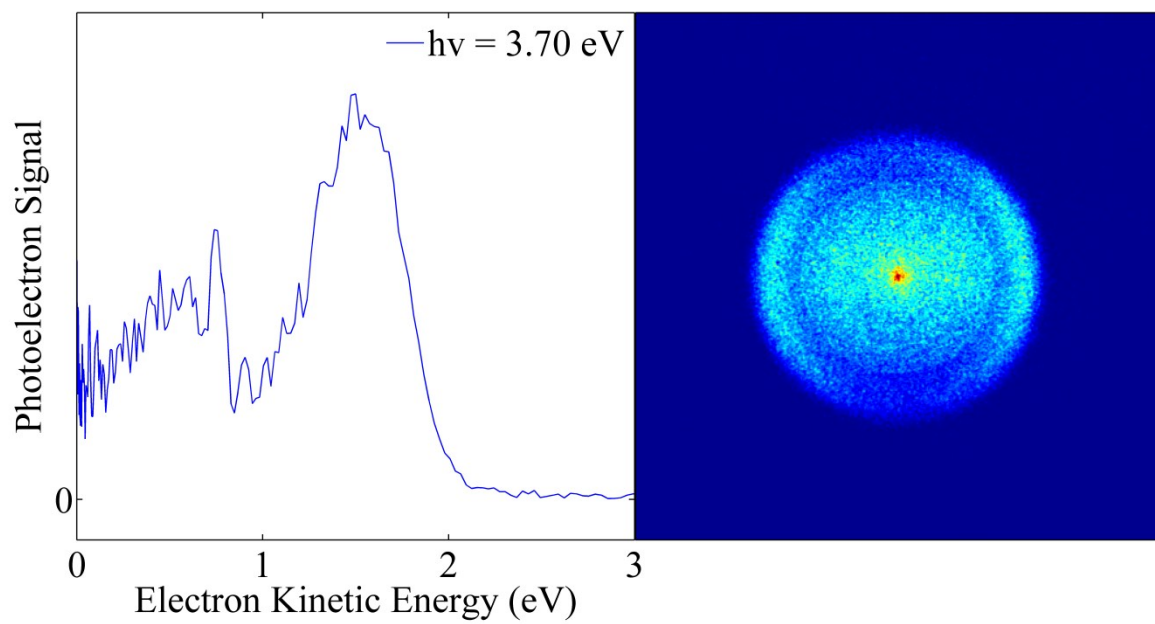
Individual photoelectron spectra and raw photoelectron images

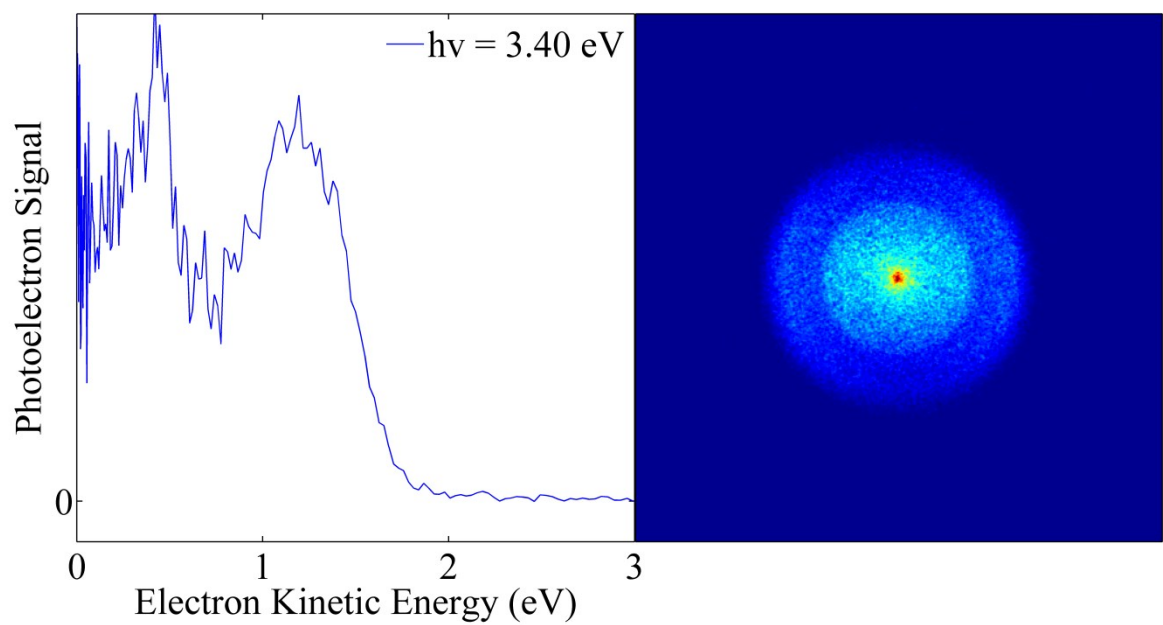
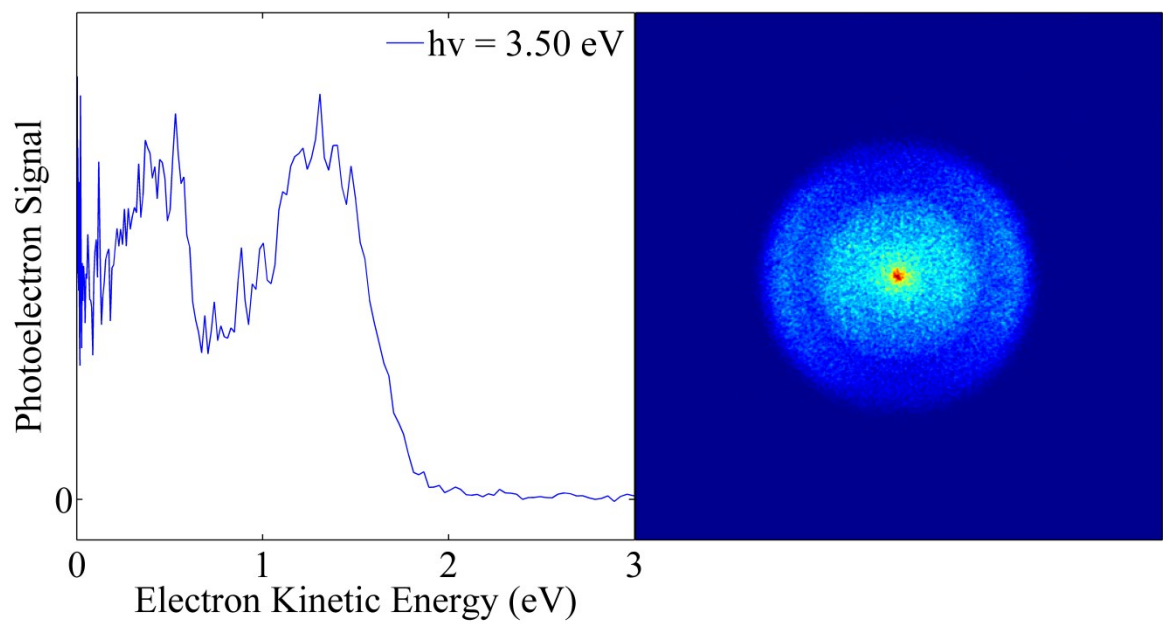
Raw photoelectron images are presented on the right of each figure. The laser polarisation is horizontal in all cases. On the right is the photoelectron spectrum obtained following polar onion peeling of the respective raw image (see main article). These together make the frequency-resolved photoelectron spectrum shown in Figure 4 of the main article.

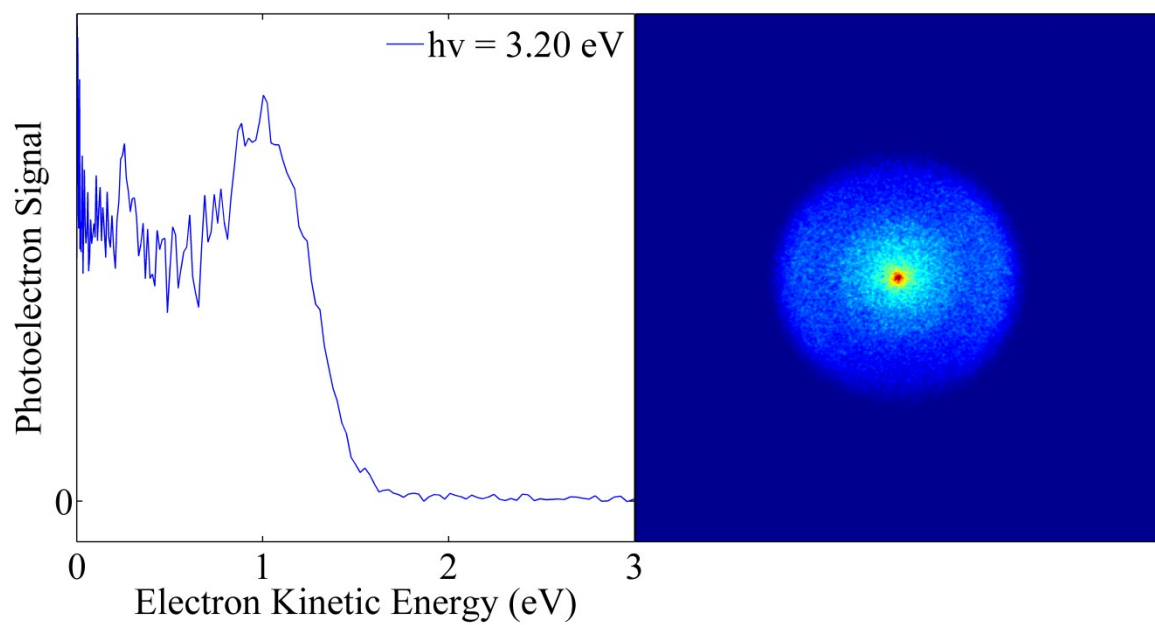
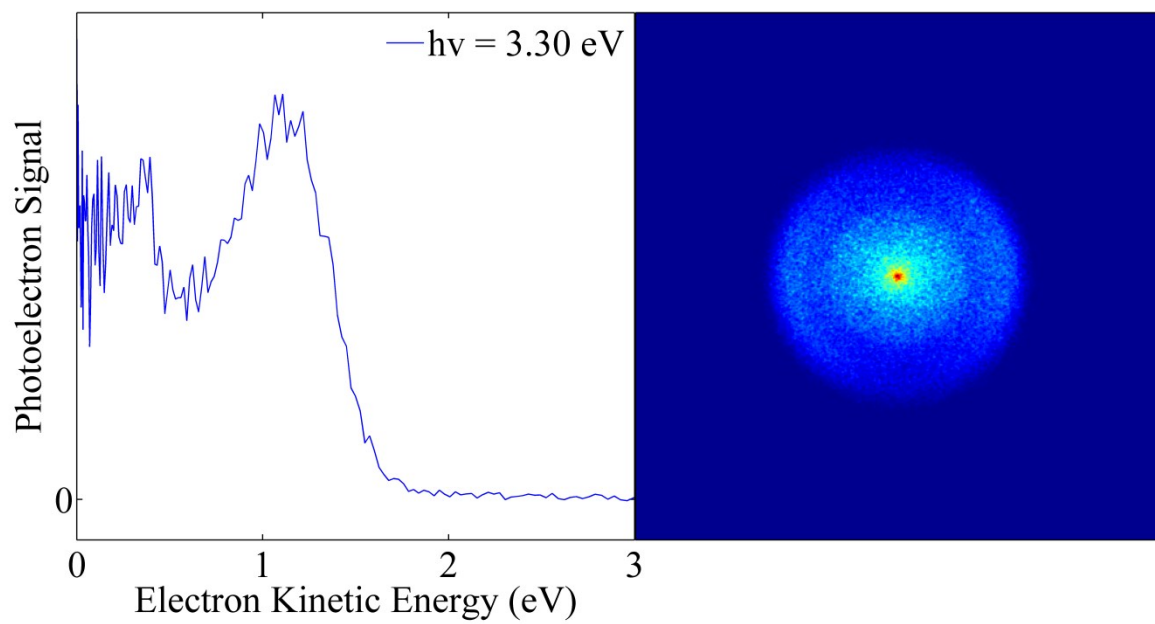
Frequency-resolved photoelectron angular distributions were also obtained and were used to generate Figure 5 in the main article.

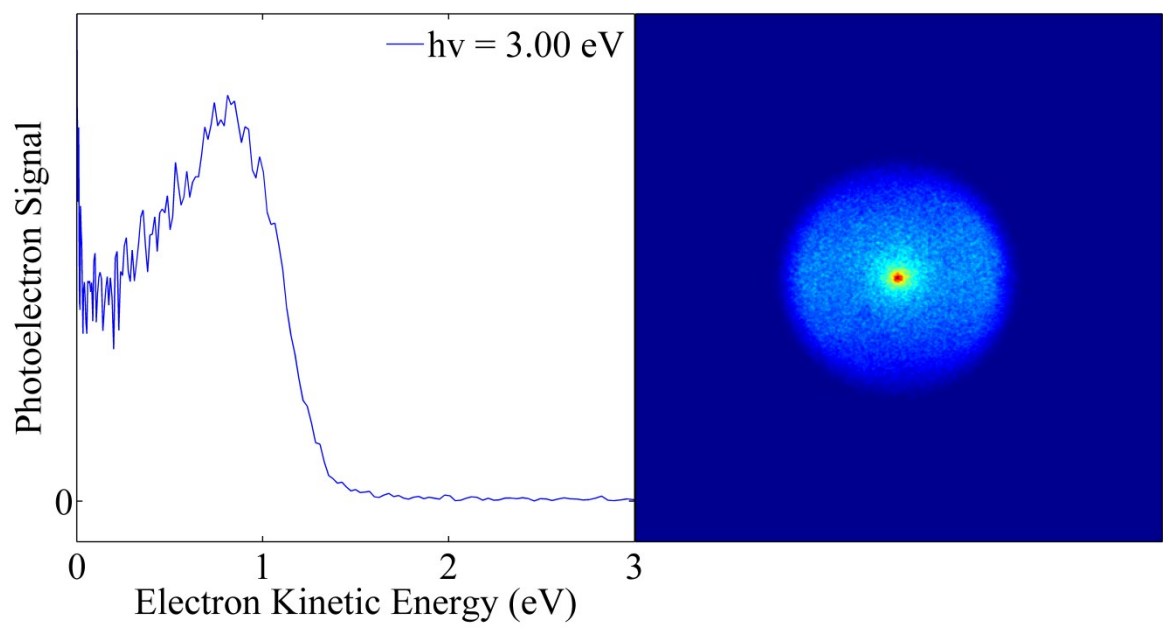
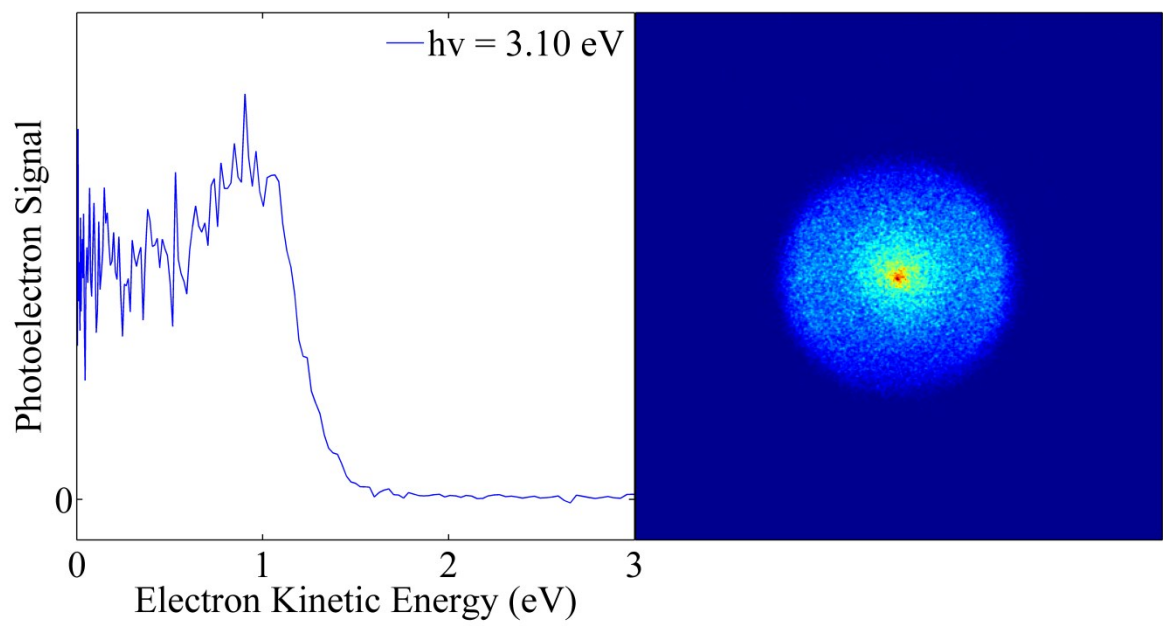


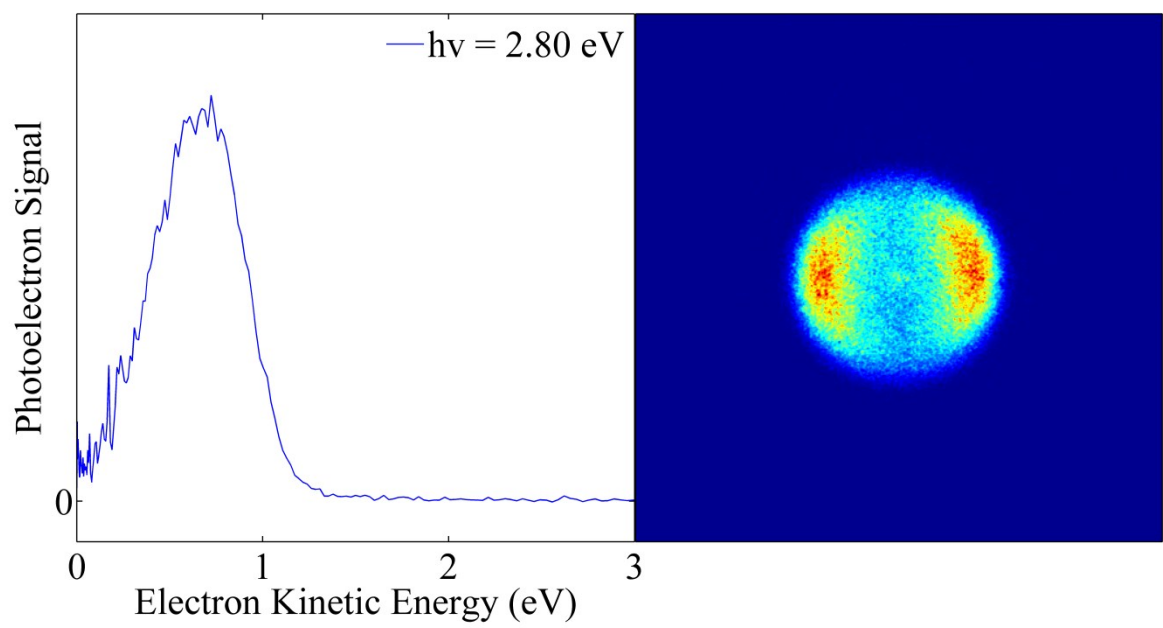
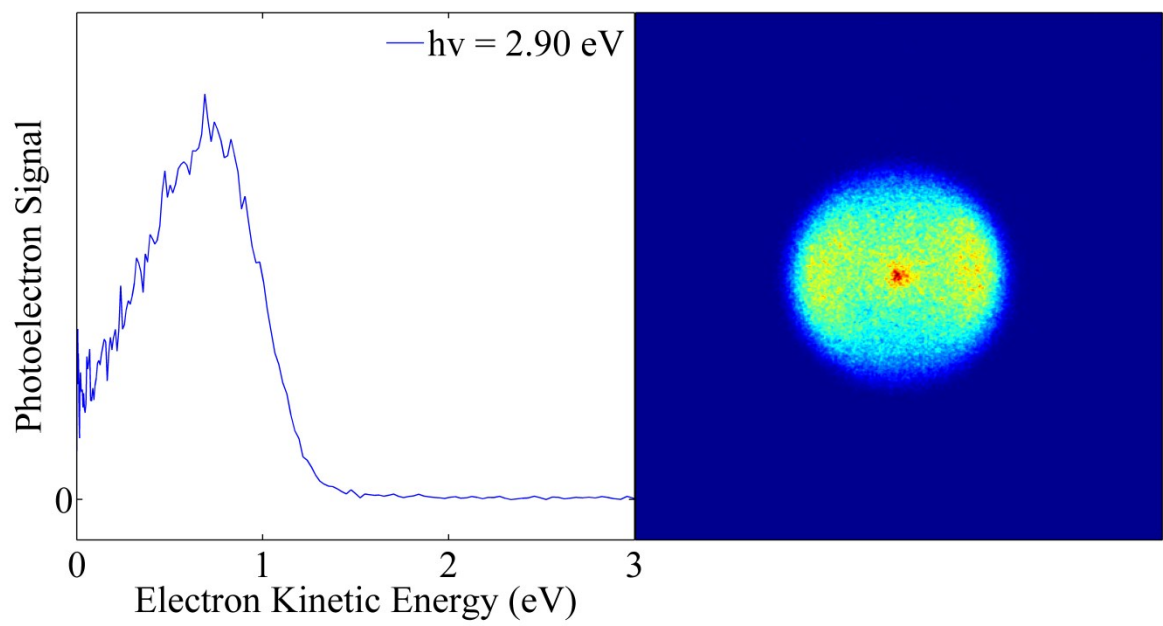


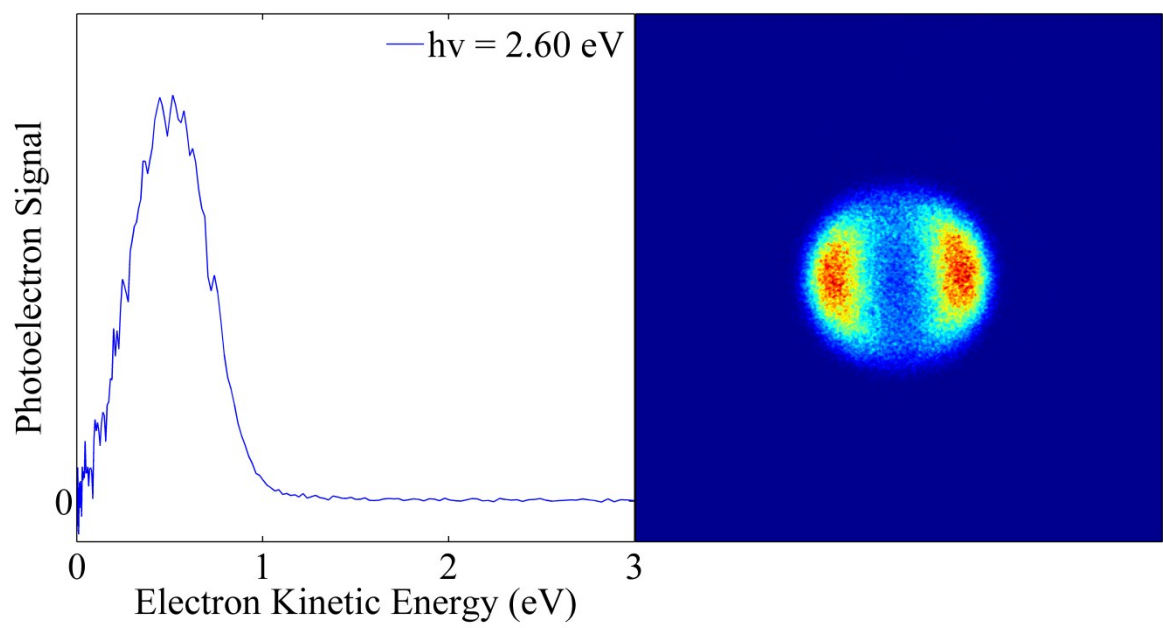
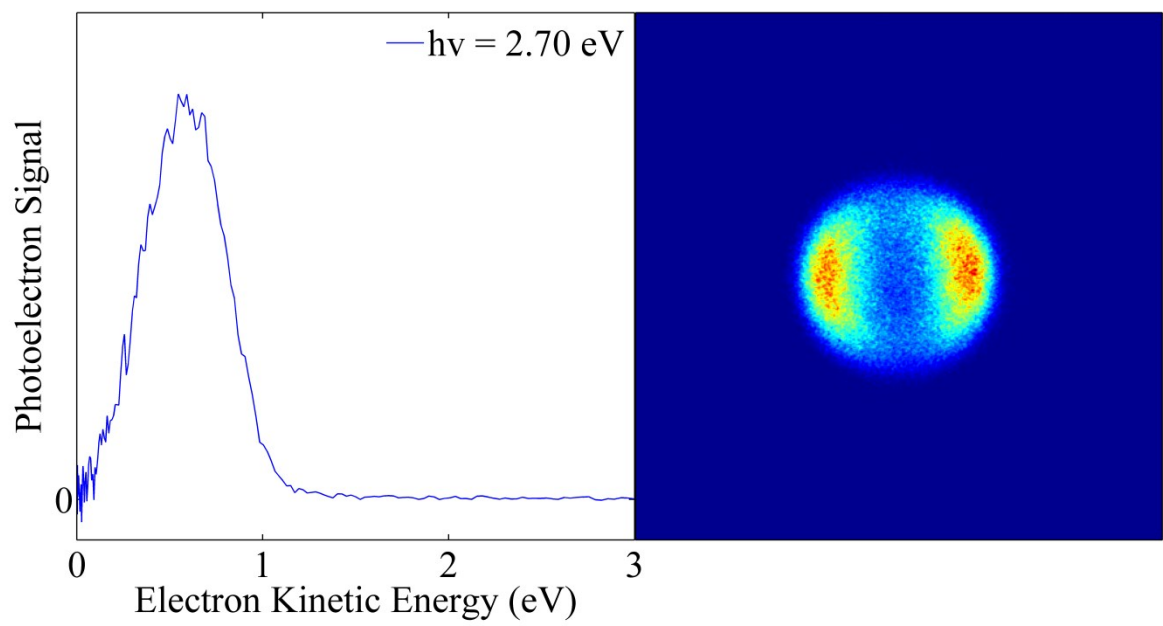


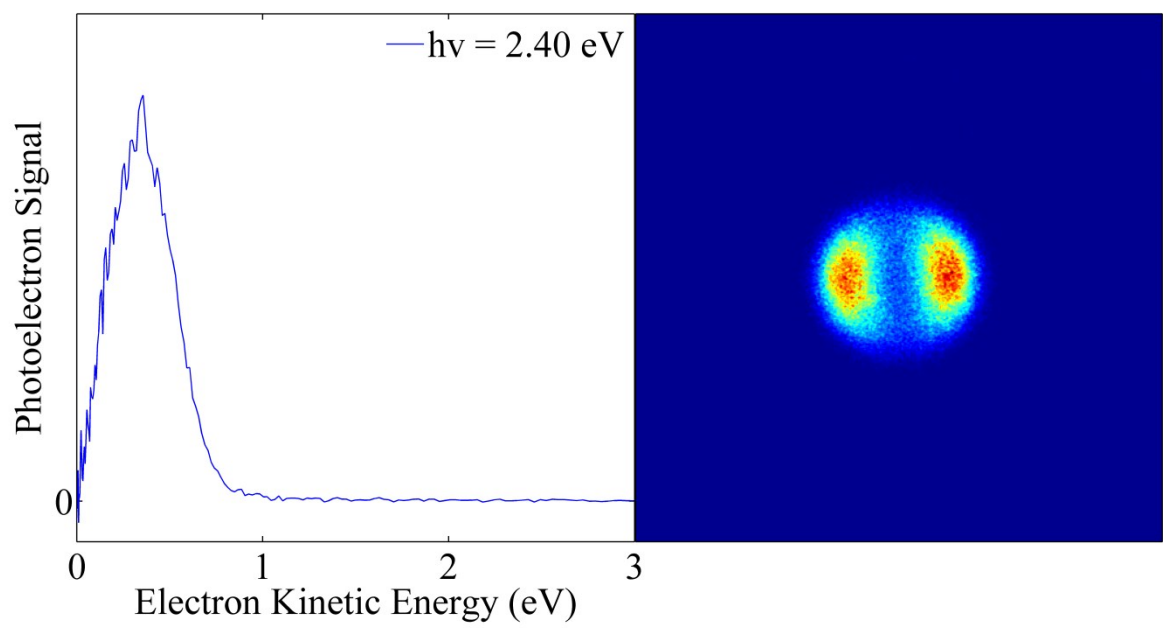
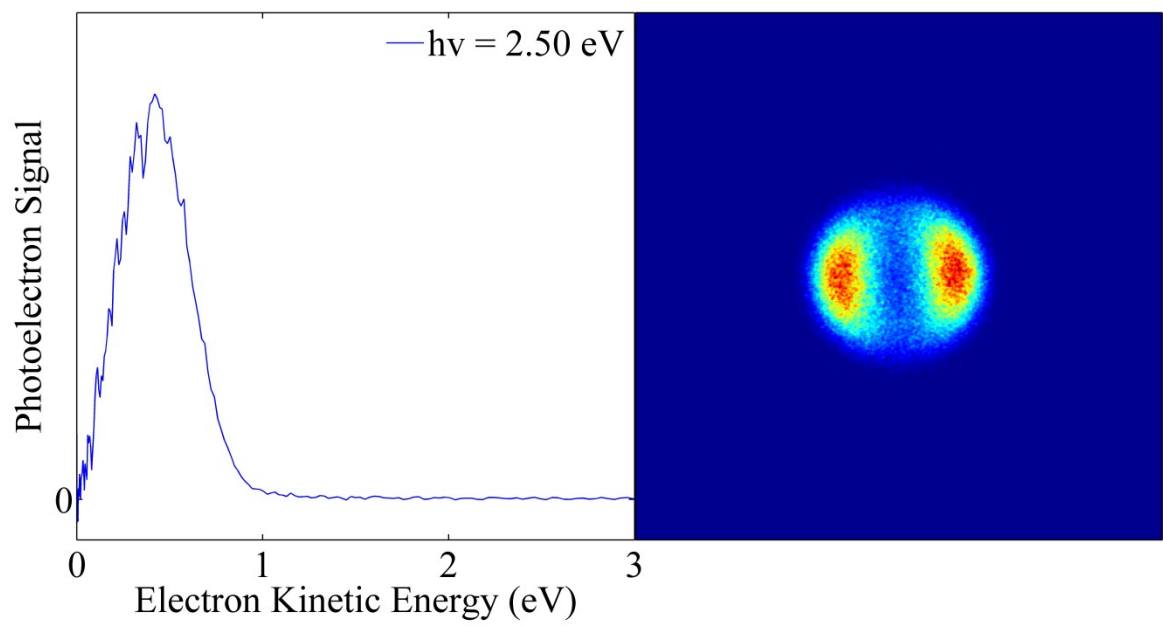


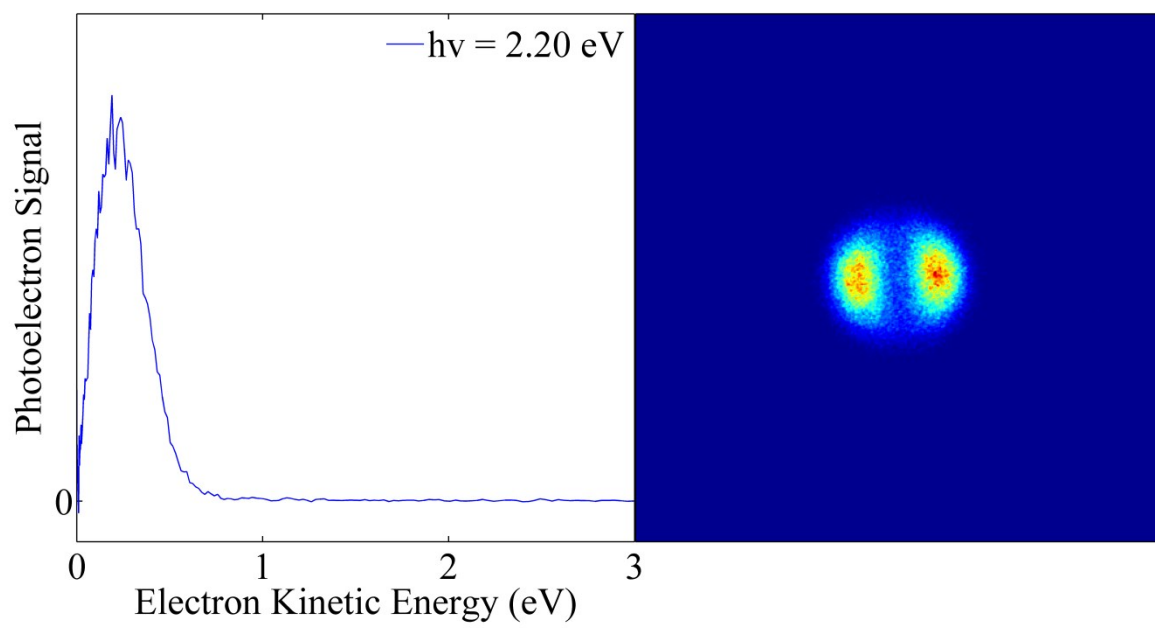
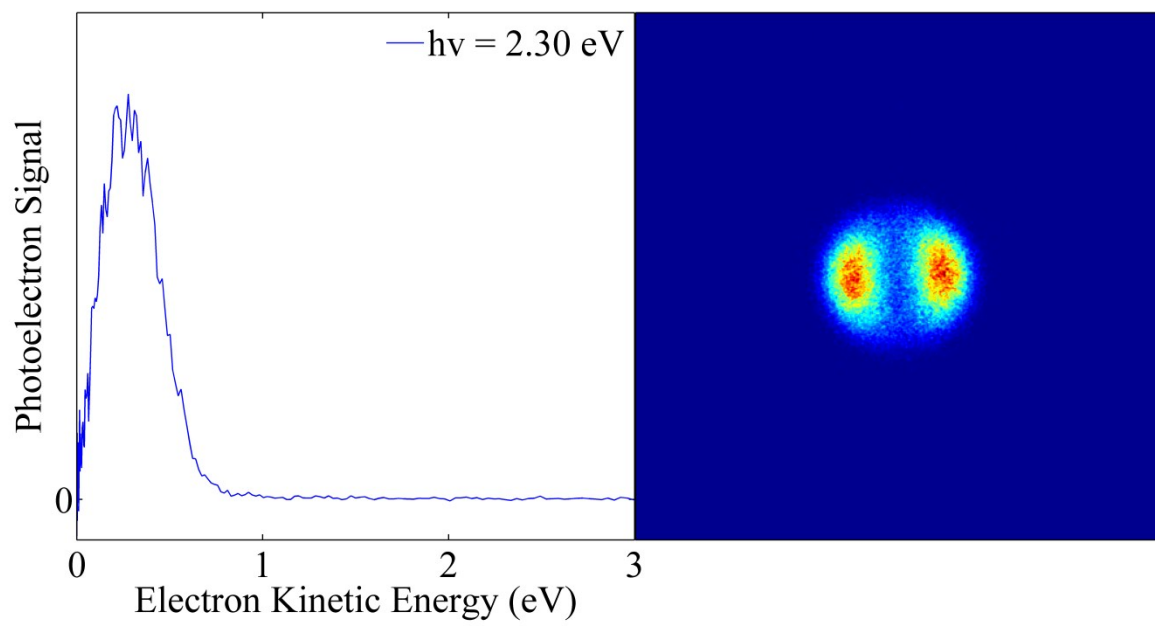


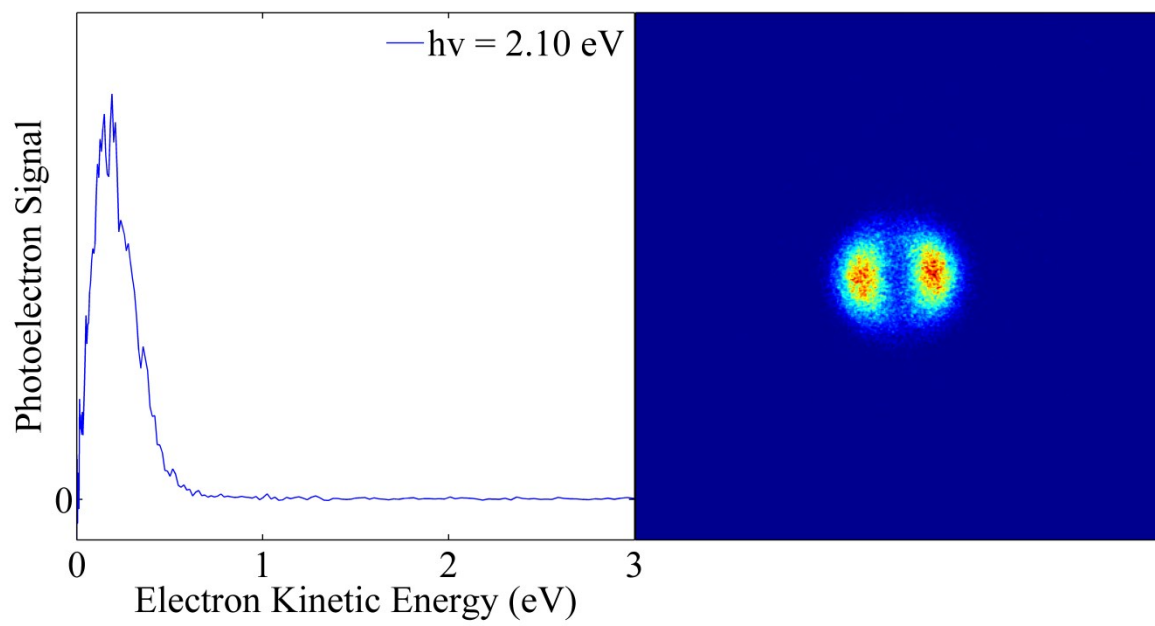






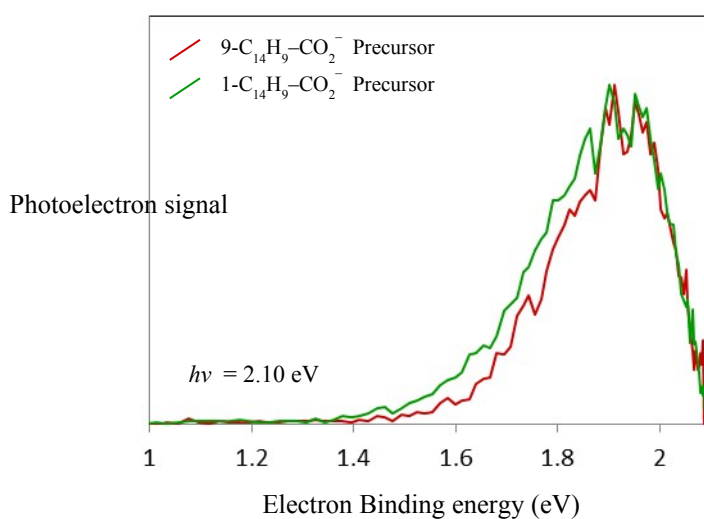






Photoelectron spectra of fragment from 9- and 1-C₁₄H₉-CO₂⁻ precursor

Photoelectron spectra taken at 2.10 eV of the *n*-C₁₄H₉⁻ fragment generated by CID of both the electrosprayed 9- and 1-C₁₄H₉-CO₂⁻ precursor anion, where the CID conditions were as mild as possible to enable photoelectron spectroscopy. The photoelectron spectrum of the CID fragment of 1-C₁₄H₉-CO₂⁻ shows is slightly lower binding energy than that of the CID fragment of 9-C₁₄H₉-CO₂⁻, but contains a significant fraction of the latter in the ion packet.

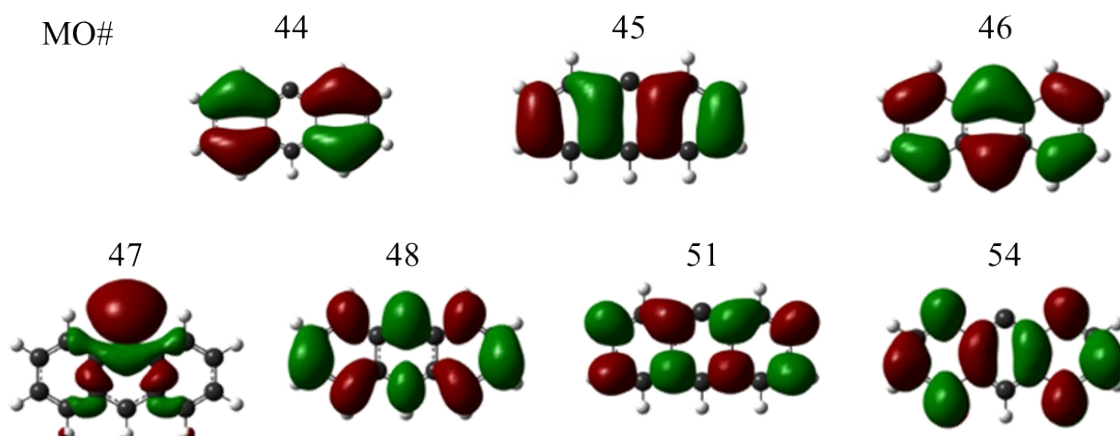


Excited state molecular orbital contributions for from 9-C₁₄H₉⁻ precursor

Orbital contributions to excited state resonances obtained from TD-DFT calculations described in main article:

$$\begin{aligned}
 (1)^1\pi\pi^* & \quad (44^2 45^2 46^1 47^2 48^1 49^0 50^0 51^0 52^0 53^0 54^0) \quad \mathbf{34\%} \\
 & \quad (44^2 45^2 46^2 47^1 48^0 49^0 50^0 51^0 52^1 53^0 54^0) \quad \mathbf{10\%} \\
 (2)^1\pi\pi^* & \quad (44^2 45^2 46^1 47^2 48^0 49^0 50^0 51^1 52^0 53^0 54^0) \quad \mathbf{34\%} \\
 & \quad (44^2 45^1 46^2 47^2 48^1 49^0 50^0 51^0 52^0 53^0 54^0) \quad \mathbf{18\%} \\
 (3)^1\pi\pi^* & \quad (44^2 45^2 46^1 47^2 48^0 49^0 50^0 51^0 52^0 53^0 54^1) \quad \mathbf{47\%}
 \end{aligned}$$

with the relevant molecular orbitals shown below.



The diffuse basis functions employed in the TD-DFT calculations (see main article) lead to significant additional contributions to the excited states of very diffuse MOs that are not associated with any valence orbitals and have therefore been omitted. By removing the diffuse function, only the contributions listed above remain, indicating that these are the predominant contributions to the resonances.